Current Status on Radiation Modeling for the Hayabusa Re-entry

Michael W. Winter
University Affiliated Research Center UARC, UC Santa Cruz

Ryan D. McDaniel, Yih-Kanq Chen, Yen Liu
NASA Ames Research Center, Moffett Field, CA 94035

David Saunders
ERC, Incorporated

Acknowledgments

Thanks to George Raiche , Aga Goodsell, and Jay Grinstead (NASA Ames) for support of the current work, as well as Peter Jenniskens (SETI) , Jim Albers (SETI), Alan Cassell (ERC Inc.), Dinesh Prabhu (ERC Inc.), Nicholas Clinton (UARC), and Jeffrey Myers (UARC) for supporting with data and information as well as everybody in the Aerothermodynamics Branch who supported in the one or the other way.
The present work was supported by NASA Contract NAS2-03/44 to UARC, UC Santa Cruz, and by NASA Contract NNA10DE12C to ERC Incorporated.

Current Status on Radiation Modeling for the Hayabusa Re-entry

Michael W. Winter
University Affiliated Research Center UARC, UC Santa Cruz

Ryan D. McDaniel, Yih-Kanq Chen, Yen Liu
NASA Ames Research Center, Moffett Field, CA 94035

David Saunders
ERC, Incorporated

Outline

- **Motivation and Methodology**
- **Numerical Procedures (DPLR, FIAT, NEQAIR)**
- **Application of the results to the Hayabusa observation mission**
- **Summary of calibration procedures**
- **Future activities**

Motivation

- Re-entry speed 11.7 km/s
  → second fastest re-entry of an artificial object
  → Peak heat flux of Hayabusa occurs at a velocity and altitude similar to Stardust
  → Important validation data for heat shield performance
- No TPS-related instrumentation aboard the capsule!
  → observation from outside.
- NASA Mission using modified DC-8
  flight altitude 12 km → no interference with clouds etc.
  but still absorption down to ~300nm in the ozone layer
- International Participants (USA, Japan, Germany, Australia) using different set-ups covering the wavelength range from 300 nm to 1600 nm with spectral resolutions between 0.2 nm and 10 nm

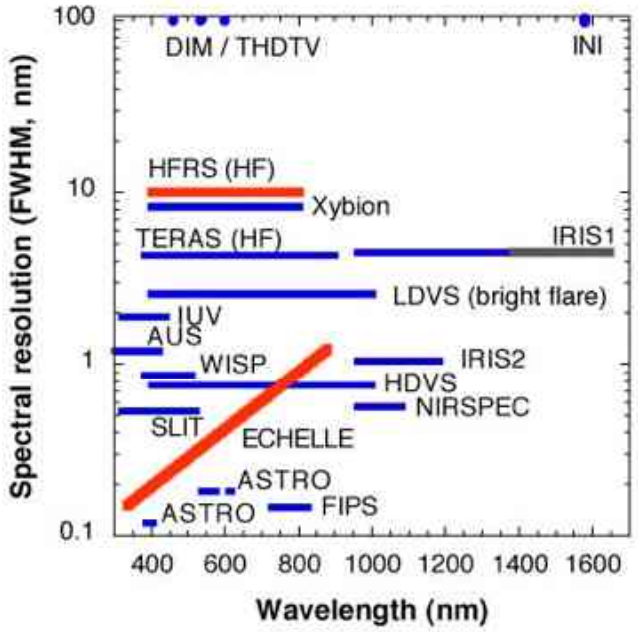

Radiation predictions are needed for:

- Pre-flight estimates of expected radiation levels
  → choice of appropriate calibration sources and signal strength
- Post-flight analysis for comparison with the experimental data
  → a baseline simulation is to be provided by NASA

Methodology

The current analysis closely followed the methods applied to the Stardust Observation (2006) by Yen Liu et al.[#] However, thermal and plasma radiation were computed separately. The following tasks were performed:

- Simulate the flow field around the capsule at selected trajectory points
  → species densities and temperatures in the flow field + radiation equilibrium wall temperatures
- Post-process the DPLR data with the material response code FIAT
  → more accurate surface temperatures
- Extract lines of sight through the plasma using view angles from trajectory simulation
- Compute spectral radiance along these lines of sight with NEQAIR
- Integrate over the lines of sight to determine total plasma radiation
- Determine effective surface areas for each axial position on the heat shield
- Compute Planck radiation according to the surface temperature distribution
- Propagate the sum of plasma and thermal radiation using the corresponding solid angle at the given trajectory point
  → incident total radiant power
- Convert received total radiant power into incident irradiance at the DC8 position.

[#] Yen Liu, Dinesh Prabhu, Kerry A. Trumble, David Saunders, and Peter Jenniskens, *Radiation Modeling for the Reentry of the Stardust Sample Return Capsule*, Journal of Spacecrafts and Rockets, Vol. 47, No. 5, September–October 2010.

DPLR

- The Data-Parallel Line Relaxation (DPLR) code is a 3-D nonequilibrium Navier-Stokes flow solver. It is one of the standard codes used by NASA for high-speed flow computations. DPLR has been validated over a wide spectrum of flight and ground-based experimental simulations.

- The DPLR code, like all Navier-Stokes flow codes, solves the equations representing the conservation of mass, momentum, and energy.

Forebody block: 81 x 121
Aftbody block: 125 x 121

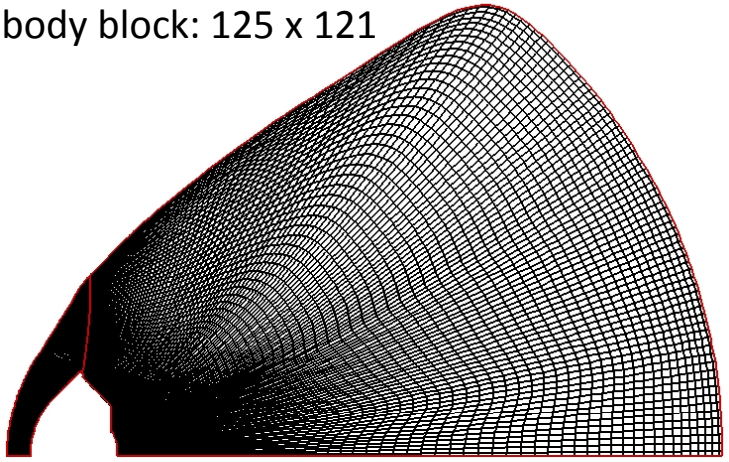

DPLR

- *DPLR* version 4.02.1 solves the full set of Navier-Stokes equations and includes the effects of finite-rate chemistry and thermal nonequilibrium.
- Axisymmetric solutions converged to steady state with global time stepping.
- Inviscid fluxes were computed using a modified Steger-Warming flux splitting. Third-order accuracy was achieved using MUSCL extrapolation with a minmod flux limiter.

Forebody block: 81 x 121
Aftbody block: 125 x 121

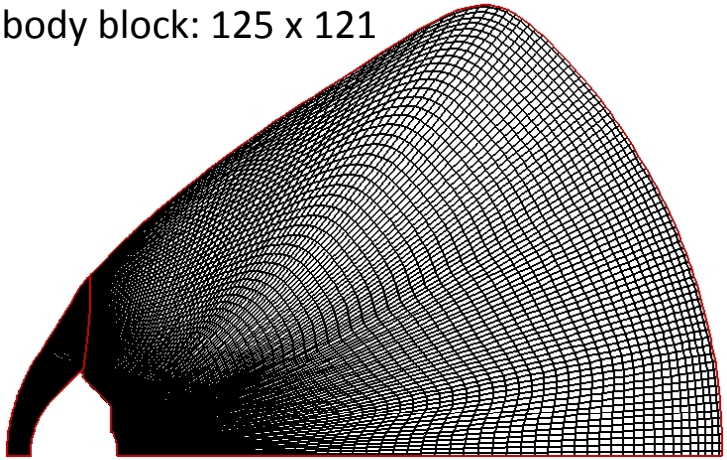

- Viscous fluxes were computed with second-order accurate central differencing.
- Park's 1990 11-species air chemistry model includes N_2, O_2, NO, NO+, N_2+, O_2+, N, O, N+, O+, e
- Fully coupled finite rate chemistry was modeled with Park's 1990 curve fits.
- A two-temperature (T and T_v) model with the vibrational temperature in nonequilibrium was used.
- Transport properties were modeled with the Yos mixing rule.
- Diffusion coefficients were modeled using the Self Consistent Effective Binary Diffusion (SCEBD) model.
- The surface was in radiative equilibrium with an emissivity value of 0.89 and fully catalytic.
- Solutions run fully laminar or fully turbulent (with Baldwin-Lomax turbulence model), with roughness induced transition predicted by Re_{kk}=100.

FIAT

Fully Implicit Ablation and Thermal Response Program*

- 1-D time-accurate solution of thermal diffusion with surface ablation and internal pyrolysis
  - Similar equations to the Aerotherm CMA code but with greater stability
- Multilayer material stack
  - TPS, adhesive, insulation, structure, air gap, etc.
  - Planar, cylindrical, or spherical geometry
  - For Hayabusa carbon phenolic was used as TPS material

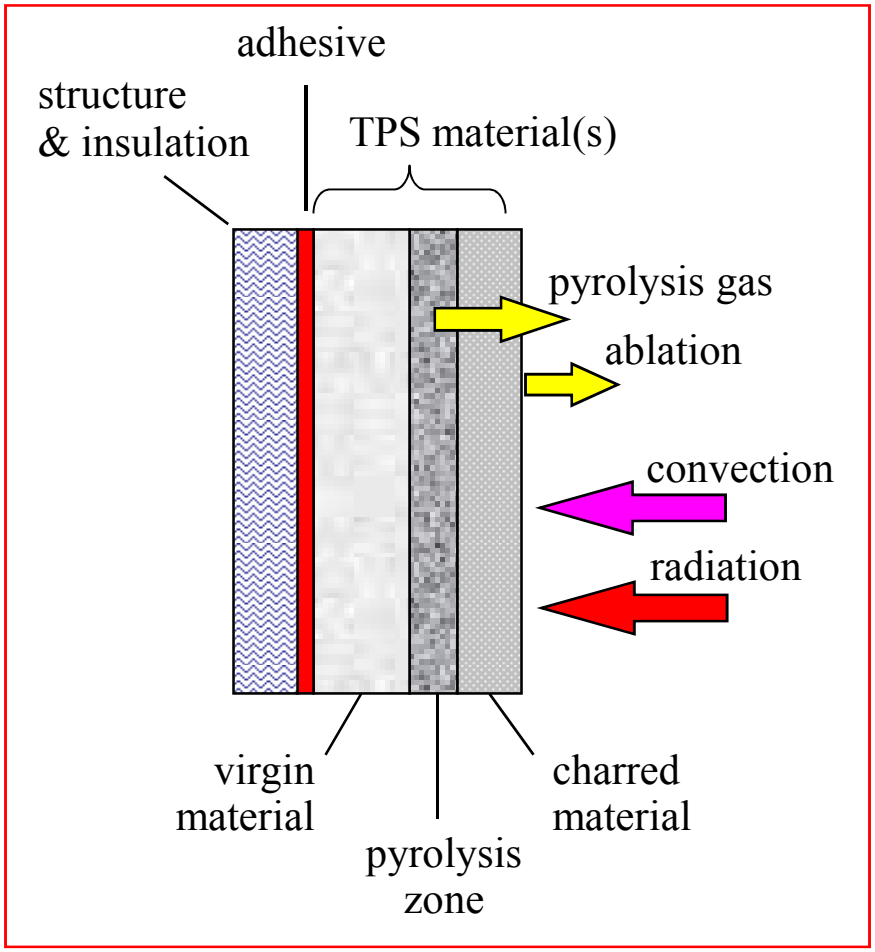

* Y.-K. Chen and F.S. Milos, "Ablation and Thermal Response Program for Spacecraft Heatshield Analysis," *Journal of Spacecraft and Rockets*, Vol. 36, No. 3, 1999, pp. 475-483.

§ C.B. Moyer and R.A. Rindal, "An Analysis of the Coupled Chemically Reacting Boundary Layer and Charring Ablator, Part II. Finite Difference Solution for the in-Depth Response of Charring Materials Considering Surface Chemical and Energy Balances," NASA CR-1061, 1968.

NEQAIR

- The Nonequilibrium Air Radiation (NEQAIR) code is a line-by-line radiation code that computes the emission and absorption spectra (along a line-of-sight) for atomic species, molecular species electronic band systems, and infrared band systems. Individual electronic transitions are evaluated for atomic and molecular species.
- The code can model the bound-free and free-free continuum radiation caused by interactions of electrons with neutral and ionized atomic species.
- Line broadenings due to Doppler, Stark, resonance, and collisional broadening as well as the natural line width are included in the code through Voigt broadening. Additional broadening (e.g. instrument broadening) can be included, in the form of both Lorentzian and Gaussian broadening.
- The radiative emission is computed along a line-of-sight. The line-of-sight is divided into a series of one-dimensional cells, and the radiative emission, absorption, and specific intensity are computed at every line-of-sight cell
- Radiative heating rate on a surface can be determined using either a tangent slab or spherical cap assumption.
- NEQAIR is capable of simulating the emission of a variety of species such as atoms (N, O, H, C, He) and molecules (N_2, N_2^+, NO, O_2, H_2, CO, C_2, CN).
However, for the present Haybusa analysis only O, N, N_2 and O_2 were used due to the wavelength range of concern and the available input from DPLR.

Trajectory information

- From DC-8 to Hayabusa: elevation and azimuth angles
- No angle of attack and rotational symmetry → only azimuth important

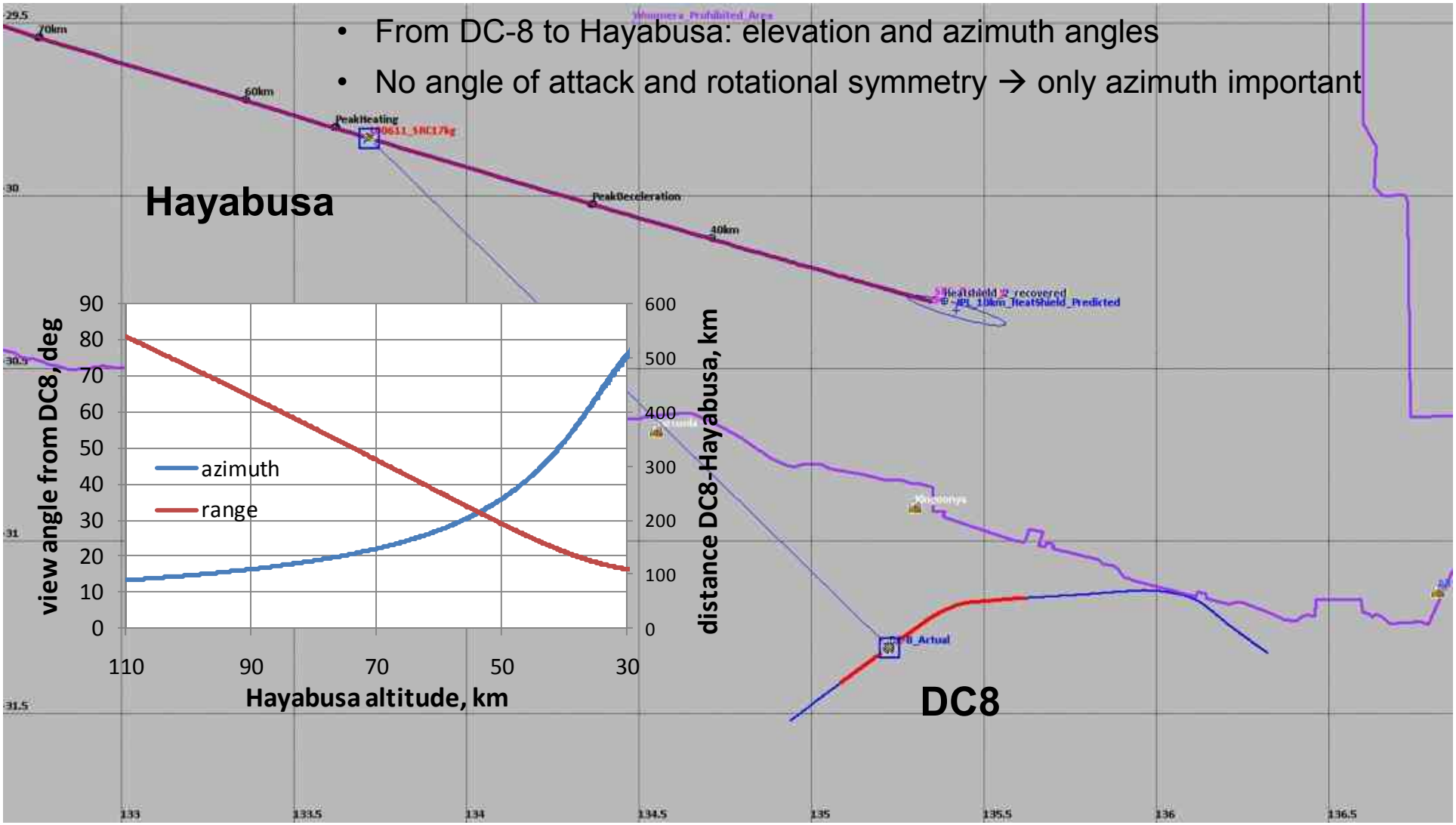

Trajectory information

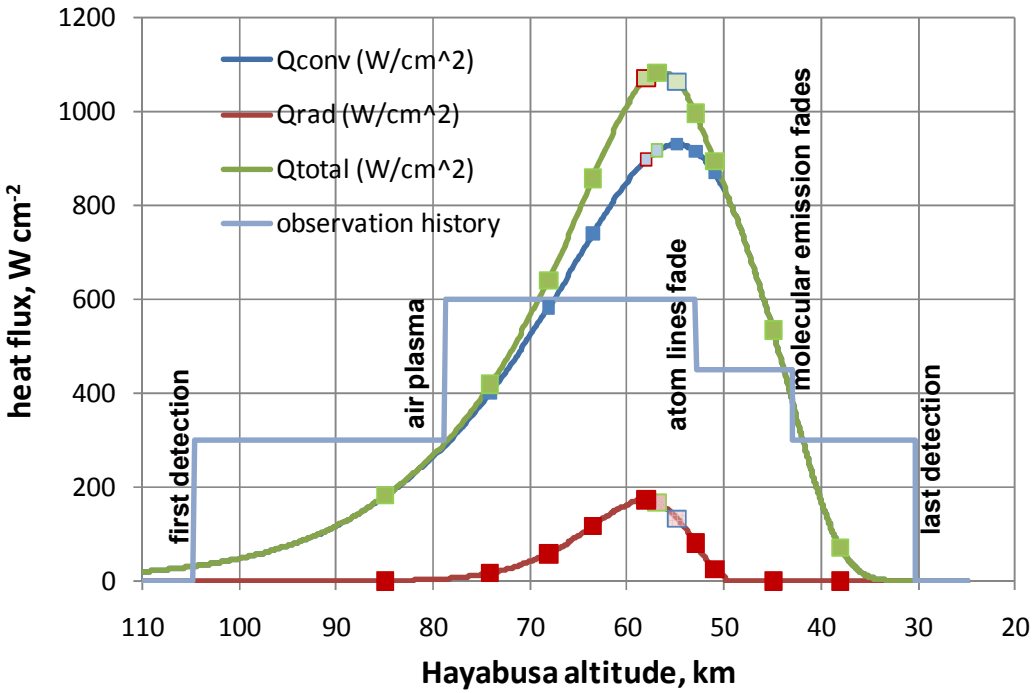

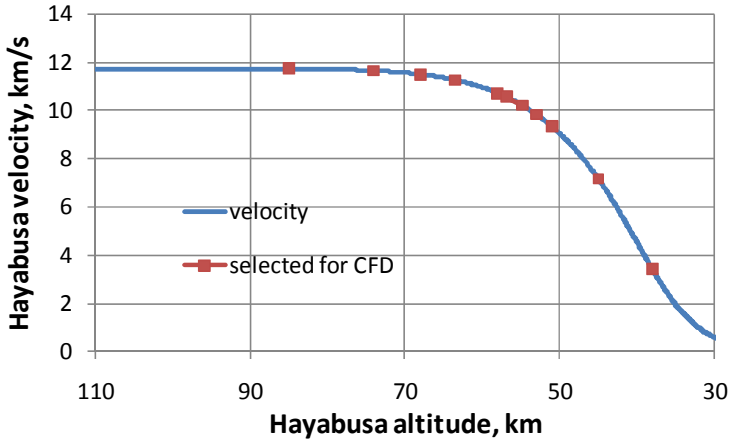

- Pre-flight, CFD solutions for radiative, convective, and total peak heating were computed.
- Post-flight, these solutions were recomputed with updated trajectory information. Four trajectory point on each side of peak heating were added with emphasis on covering the range where spectroscopic data was measured.
- The maximum altitude for CFD was chosen to be 85km which is considered the limit for a continuum flow.

Trajectory information

Selected trajectory points:

point	UTC	altitude	lam/turb	view angle	range	$T_{surf,stag}$	
1	13:52:03.8	85 km	lam	17.5 deg	398.9 km	1050 K	
2	13:52:03.8	74 km	lam	20.6 deg	334.8 km	1816 K	
3	13:52:03.8	68 km	lam	22.9 deg	299.3 km	2419 K	
4	13:52:03.8	63.5 km	lam	25.2 deg	272.5 km	2839 K	
5	13:52:03.8	58 km	turb	28.6 deg	239.9 km	3143 K	$q_{rad,max}$
6	13:52:03.8	56.9 km	turb	29.4 deg	233.3 km	3167 K	**$q_{tot,max}$**
7	13:52:03.8	54.9 km	turb	31.0 deg	221.5 km	3206 K	$q_{conv,max}$
8	13:52:03.8	53 km	turb	32.7 deg	210.6 km	3199 K	
9	13:52:03.8	51 km	turb	34.7 deg	199.1 km	3190 K	
10	13:52:03.8	45 km	turb	42.6 deg	166.1 km	2961 K	
11	13:52:03.8	38 km	turb	56.2 deg	133.1 km	1991 K	

DPLR results

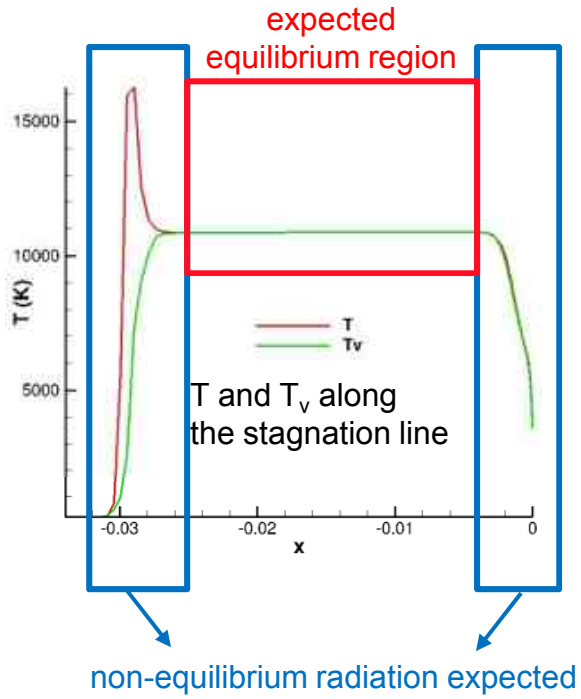

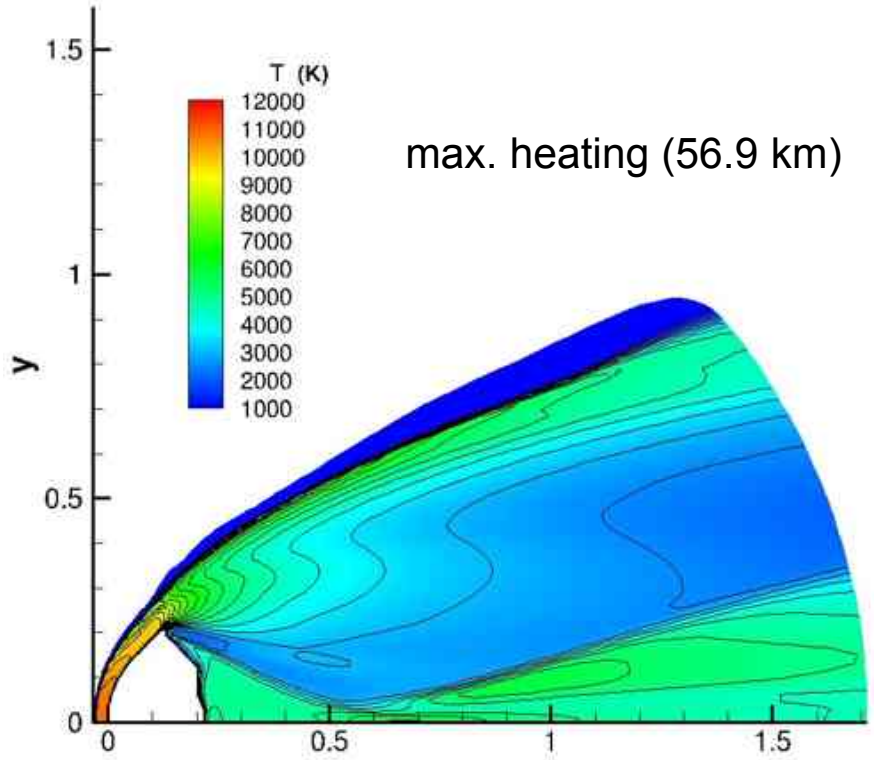

max. heating (56.9 km)

- The DPLR solution gives radiation equilibrium surface temperatures and nonequilibrium flow field data
- The temperatures along the stagnation line show a distinct plateau which indicates the equilibrium region behind the shock.
- To determine the loads on the heat shield, only the forebody solution is necessary, but lines of sight under a given view angle require the wake as well.

DPLR results

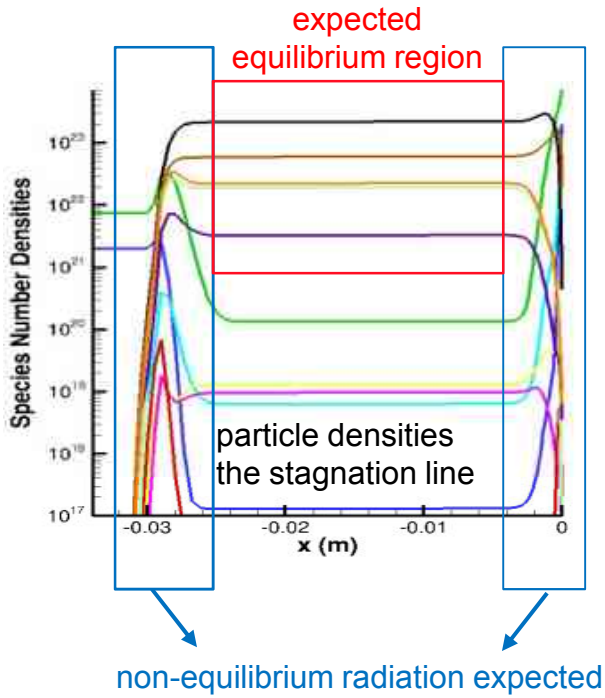

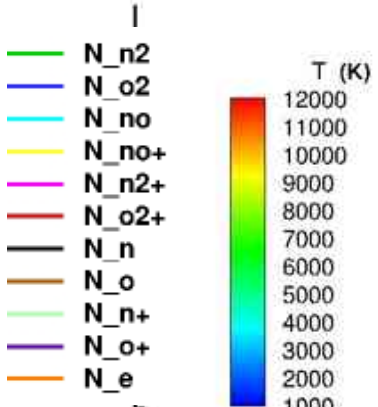

max. heating (56.9 km)

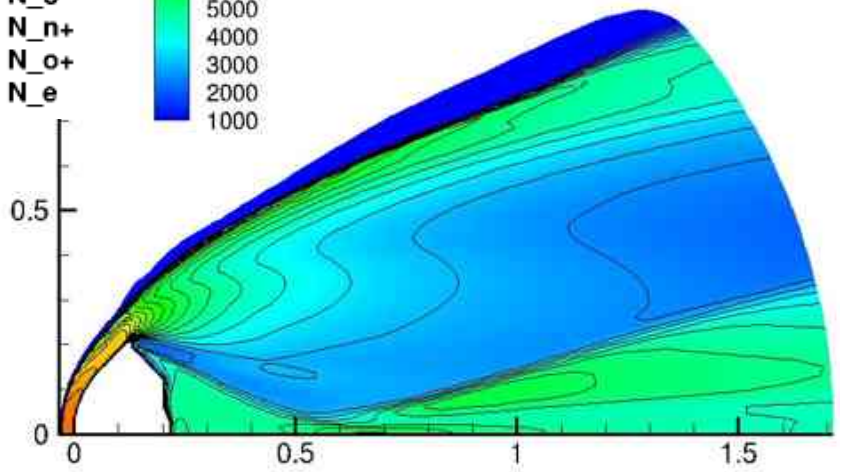

- The DPLR solution gives radiation equilibrium surface temperatures and nonequilibrium flow field data
- The temperatures along the stagnation line show a distinct plateau which indicates the equilibrium region behind the shock.
- To determine the loads on the heat shield, only the forebody solution is necessary, but lines of sight under a given view angle require the wake as well.

Extraction of lines of sight

- Generate 3d flow field by rotating the 2d flow solution.
- Create a uniform 2d orthogonal grid perpendicular to the view angle vector behind the flow field
- Generate lines of sight for each grid element: determine intersections with flow field outer boundary and capsule surface, and eliminate “empty” line segments.

- Due to the large distance to the observer, parallel lines are sufficient.
- lines are cut off in the wake at a specified distance from the body (0.1 x capsule length).

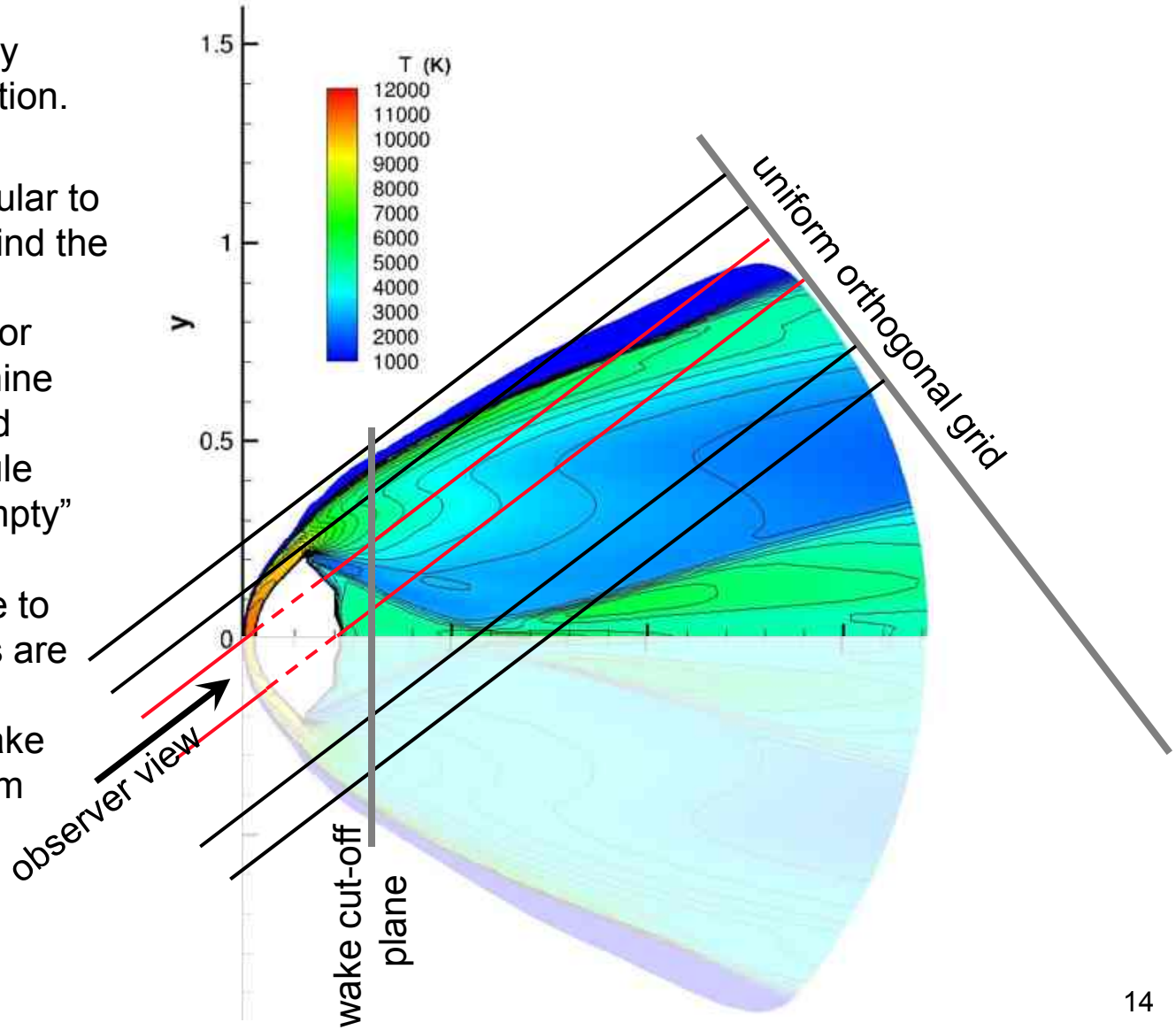

Extraction of lines of sight

- Generate 3d flow field by rotating the 2d flow solution.
- Create a uniform 2d orthogonal grid perpendicular to the view angle vector behind the flow field
- Generate lines of sight for each grid element: determine intersections with flow field outer boundary and capsule surface, and eliminate “empty” line segments.

- Due to the large distance to the observer, parallel lines are sufficient.
- lines are cut off in the wake at a specified distance from the body (0.1 x capsule length).

Lines of sight for:

74km, 20.6 deg

53km, 32.7 deg

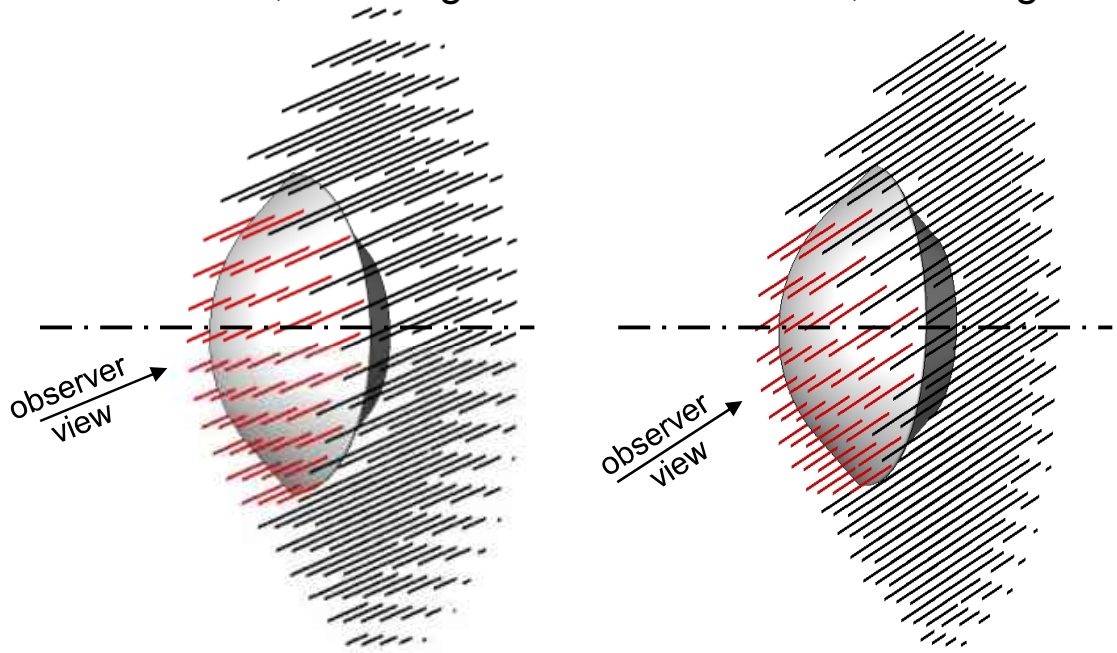

In average, 47 **inner** and 112 **outer** lines of sight were computed in the half space of the flow field for each trajectory point.

Finally: Interpolate flow field data along these lines and convert to NEQAIR input.

Radiation Transport

- Both plasma and surface radiation are computed in spectral radiance values i.e. power per emitting surface, wavelength interval and solid angle in the units W m^{-2} nm^{-1} sr^{-1} .
- Along the trajectory, the effective emitting surface will change due to the changing view angle and the solid angle will vary with the distance to the observer.
- Therefore, a calibration of the instruments to spectral radiance cannot be performed in a straightforward way and the emitted radiance has to be converted to spectral irradiance (received power per receiving surface in the units W m^{-2} nm^{-1})
- For this purpose, all computed spectral radiance values will be converted to a spectral radiant flux in W/nm by multiplying with the emitting surface and the solid angle in which radiation is emitted and then divided by the receiving surface given by the smallest aperture in the detection set-up. (The aperture diameter finally cancels out since it is used both for the solid angle and the receiving surface.)
- Needed quantities:
  distance Hayabusa-DC8, emitting surface area (grid cell for plasma, projected Hayabusa surface for thermal radiation), view angle.
- The same procedure was applied to the calibration sources.

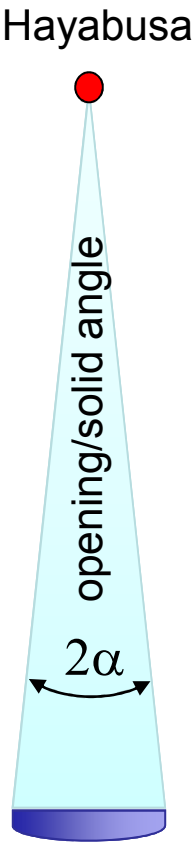

$$\Omega = 2\,\pi\,(1-\cos(\alpha))$$

Radiation Transport

- The detected radiation has been partly absorbed by the atmosphere.
- During pre-flight analysis the atmospheric extinction was computed with Modtran for different Hayabusa altitudes and used for the design of the calibration set-up.
- However, extinction will not be taken into account for the radiation predictions since it is supposed to be included in the individual calibration for each experiment.

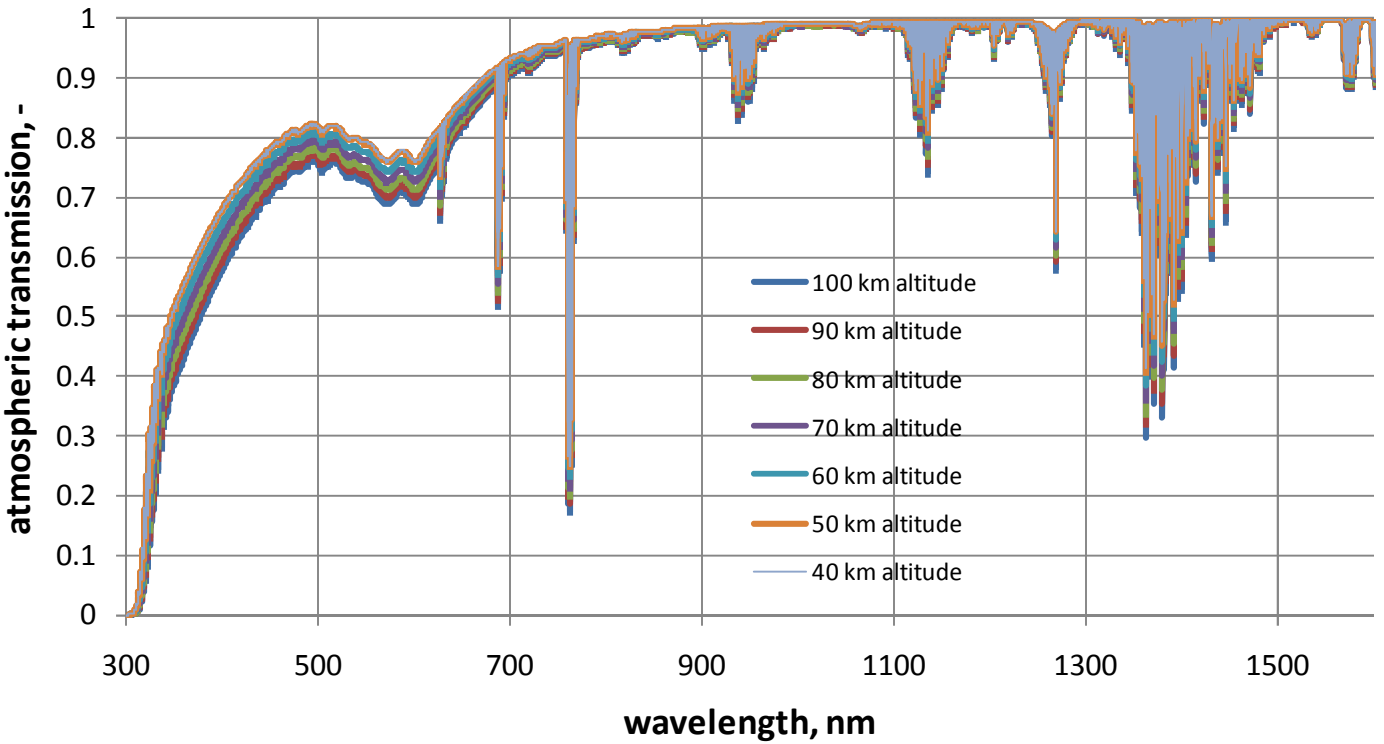

NEQAIR Results

- NEQAIR runs were performed on all lines of sight for N, O, N2 and N2+ as the main radiating species in the wavelength range between 300nm and 1500nm
- Parameters: initial resolution 0.01nm, integrated to 0.1nm and broadened to 0.3nm with Boltzmann excitation and Quasi-Steady State (QSS) assumption in separate r

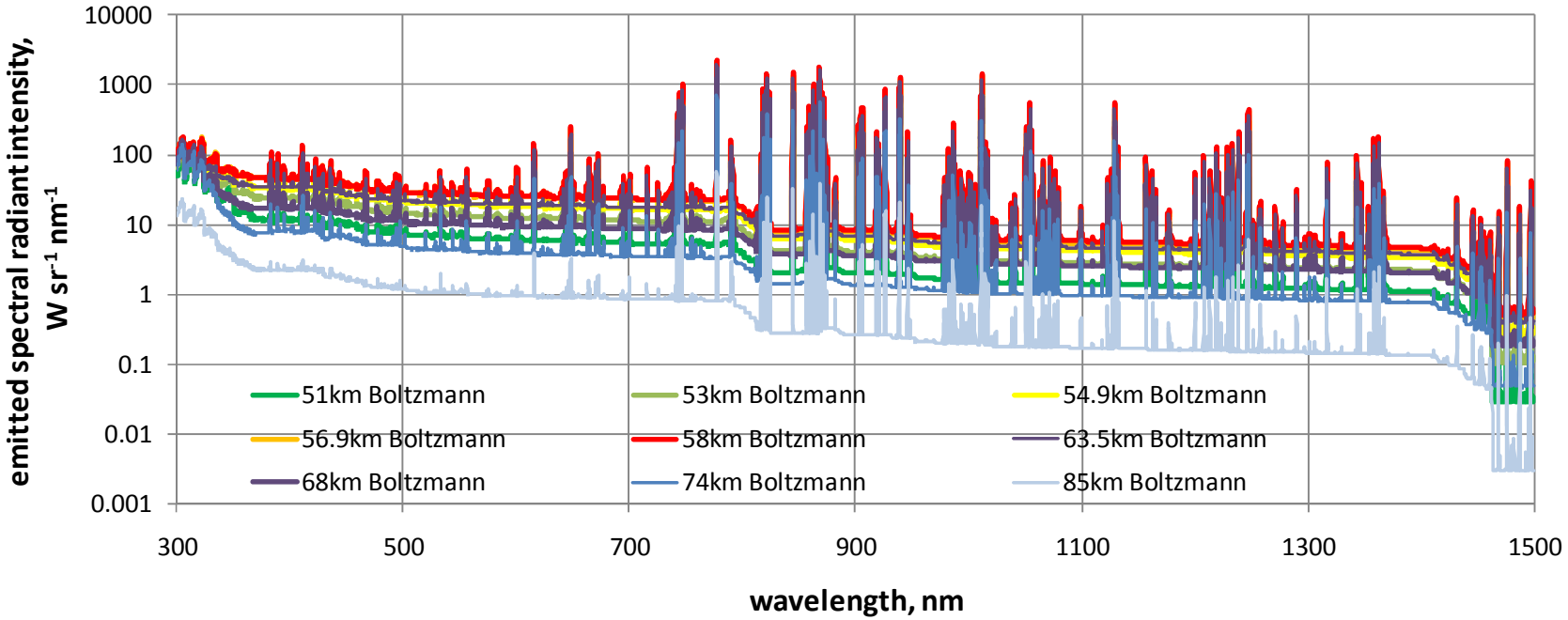

- Strongest emission peaks from atomic lines.
- Strongest spectra are obtained at 58km (which was the predicted altitude for maximum radiative heating).

NEQAIR Results

- NEQAIR runs were performed on all lines of sight for N, O, N_2 and N_2^+ as the main radiating species in the wavelength range between 300nm and 1500nm
- Parameters: initial resolution 0.01nm, integrated to 0.1nm, and broadened to 0.3nm with Boltzmann excitation and Quasi-Steady State (QSS) assumption in separate runs.

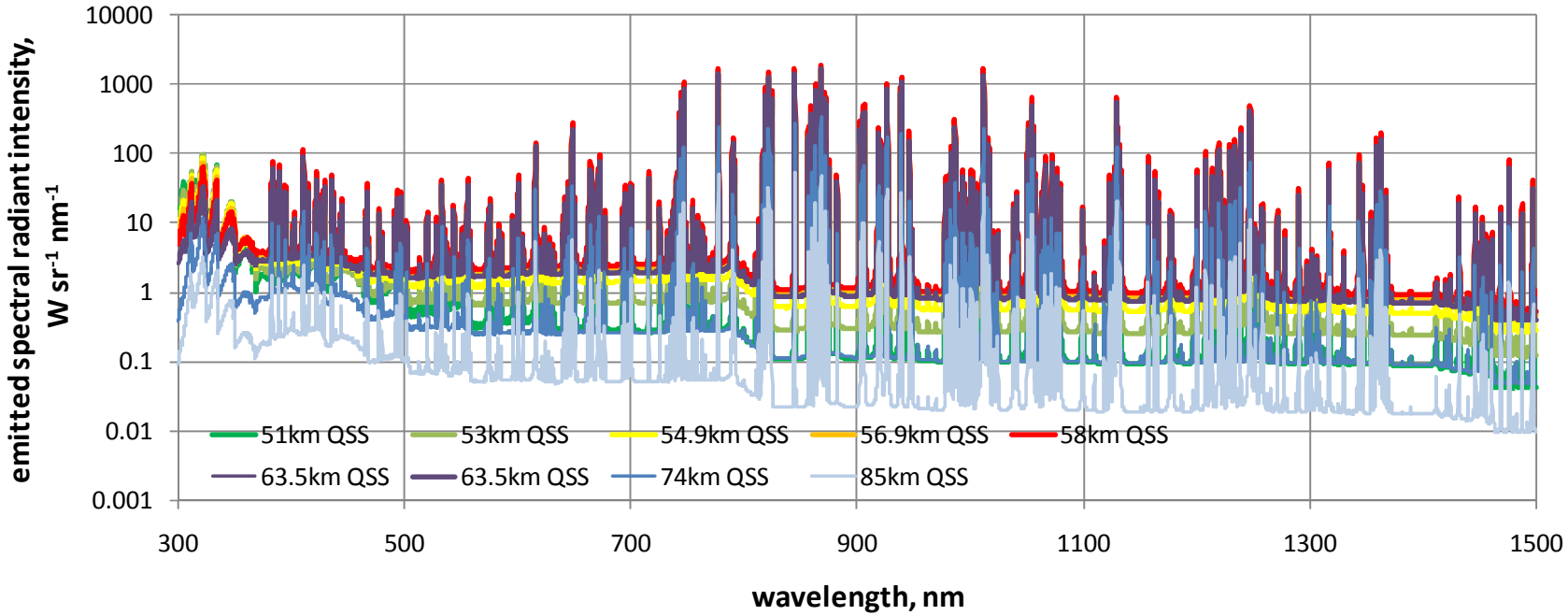

- QSS yields almost the same atomic line peak values but significantly lower continuum and molecule emission.

Thermal Radiation

- As seen during the Stardust observation, a major part of the emitted radiation is thermal emission from the glowing heat shield.
- This radiation is computed as Planck radiation. An emissivity value of 0.9 (charred carbon phenolic) was used.
- The spectral radiance has to be integrated over the surface area to obtain the total radiation which is observed.

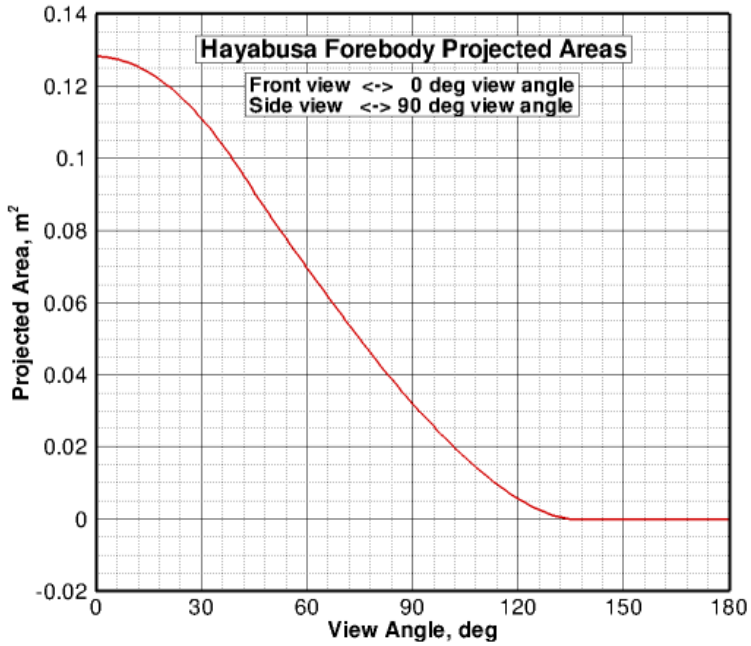

- Since the capsule approaches the observer, the view angle to the surface changes continuously. For the surface radiation, only the projected area can be used due to Lambert's Law.
- For a computation of the projected area, a Fortran code developed for the Stardust observation was applied to the Haybusa forebody.

Effective (projected) surface areas

- To be able to account for temperature gradients, the projected areas were computed on the CFD surface grid for each circular ring of cells.
- The back shell was assumed to emit only negligible contributions to the total radiation.

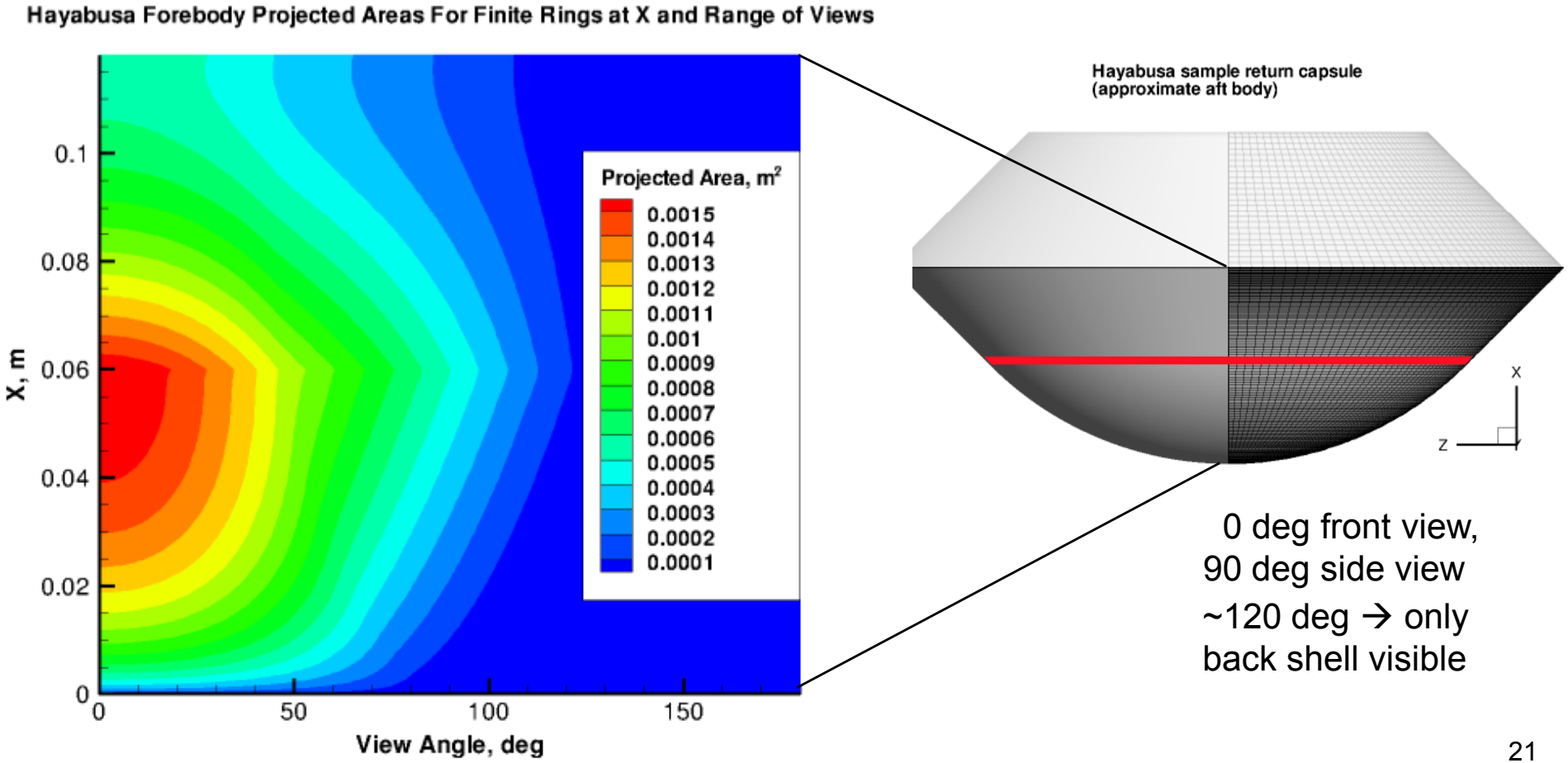

0 deg front view,
90 deg side view
~120 deg → only back shell visible

Surface Temperatures

- The FIAT computations were performed for 25 points along the surface, the resulting temperatures have been interpolated back onto the 146 cells of the DPLR surface grid to perform the radiation computation.
- Through material response, the temperature profiles show higher gradients across the surface for the laminar cases and flatten for the turbulent ones.
- The temperatures are significantly reduced, except for the two trajectory points after convective peak heating which show only a moderate change.

DPLR: radiation equilibrium

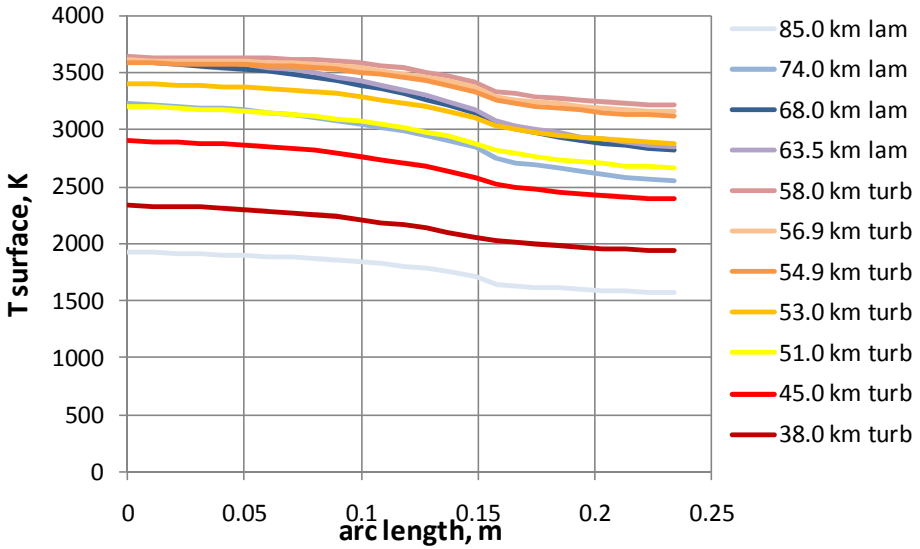

FIAT: material response

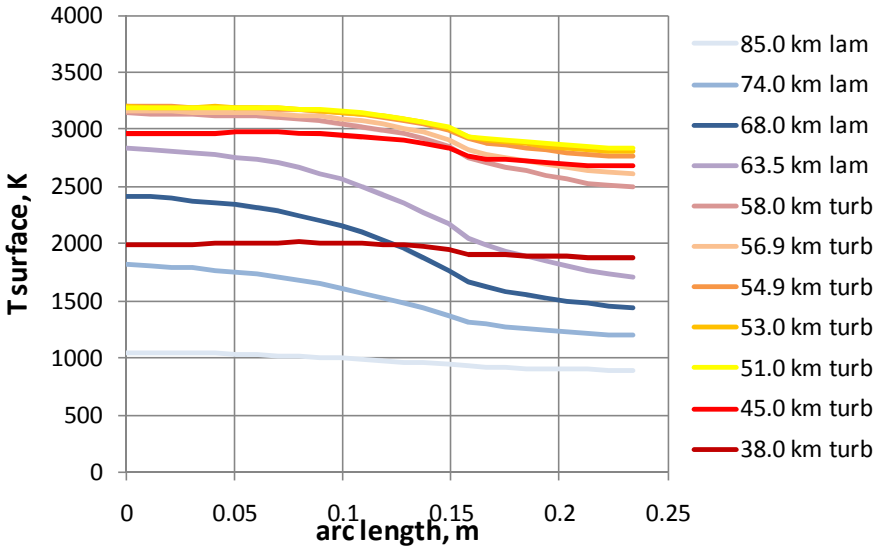

Thermal Radiation

- The thermal radiation is computed as Planck radiation. An emissivity value of 0.9 (charred carbon phenolic) was used.

$$L_\lambda(T) = \varepsilon_\lambda \frac{2hc^2}{\lambda^5} \frac{1}{\exp\left(\frac{hc}{\lambda kT}\right) - 1}$$

- The spectral data were converted from emitted spectral radiance to spectral irradiance received at the DC-8 position.
- A significant increase in continuum radiation can be seen between 74 km and 68 km altitude.
- The maximum of incident thermal radiation occurs at an altitude of 51 km clearly after peak heating.

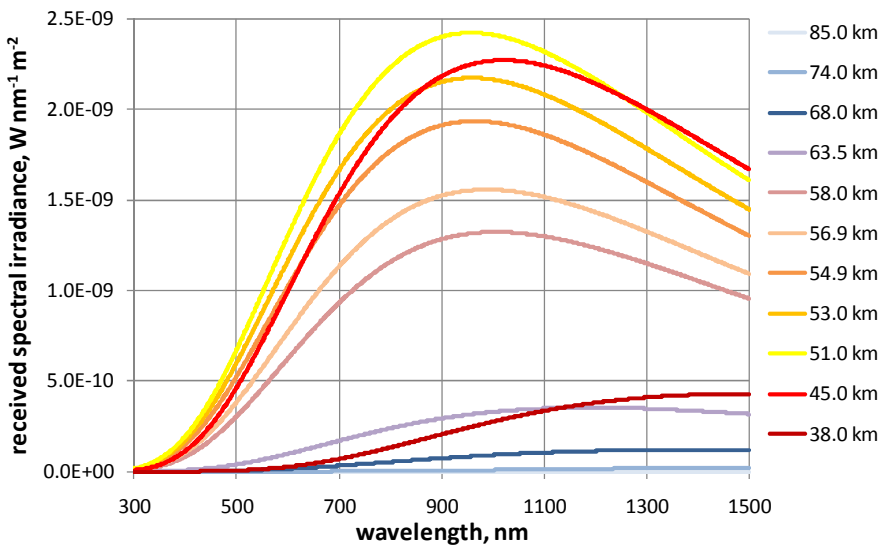

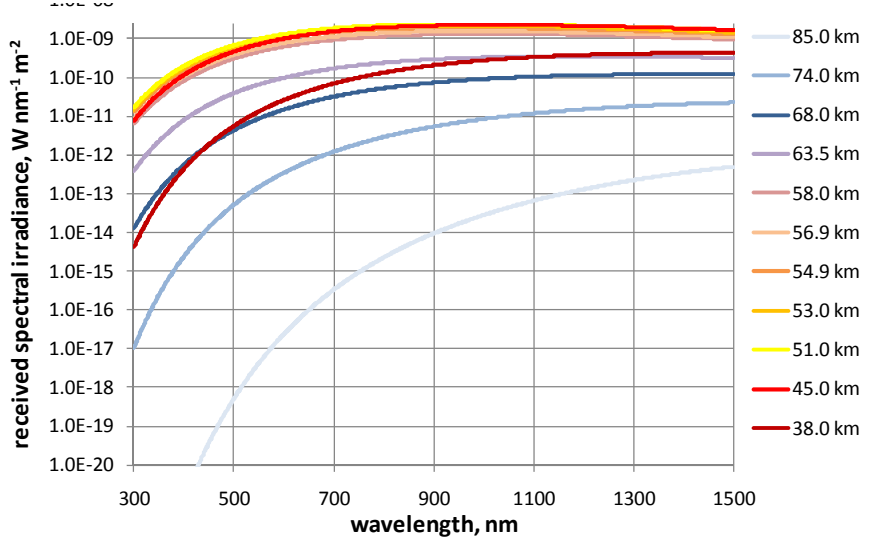

Incident Radiation

- The total incident radiation at the DC-8 position is given by the superposition of thermal and plasma emission.
- The atom line emission of the plasma increases up to peak radiative heating and starts fading out after peak heating. After that point, the spectra are dominated by continuum emission. The molecular emission (mainly N_2^+), however, keeps increasing down to 51km altitude.

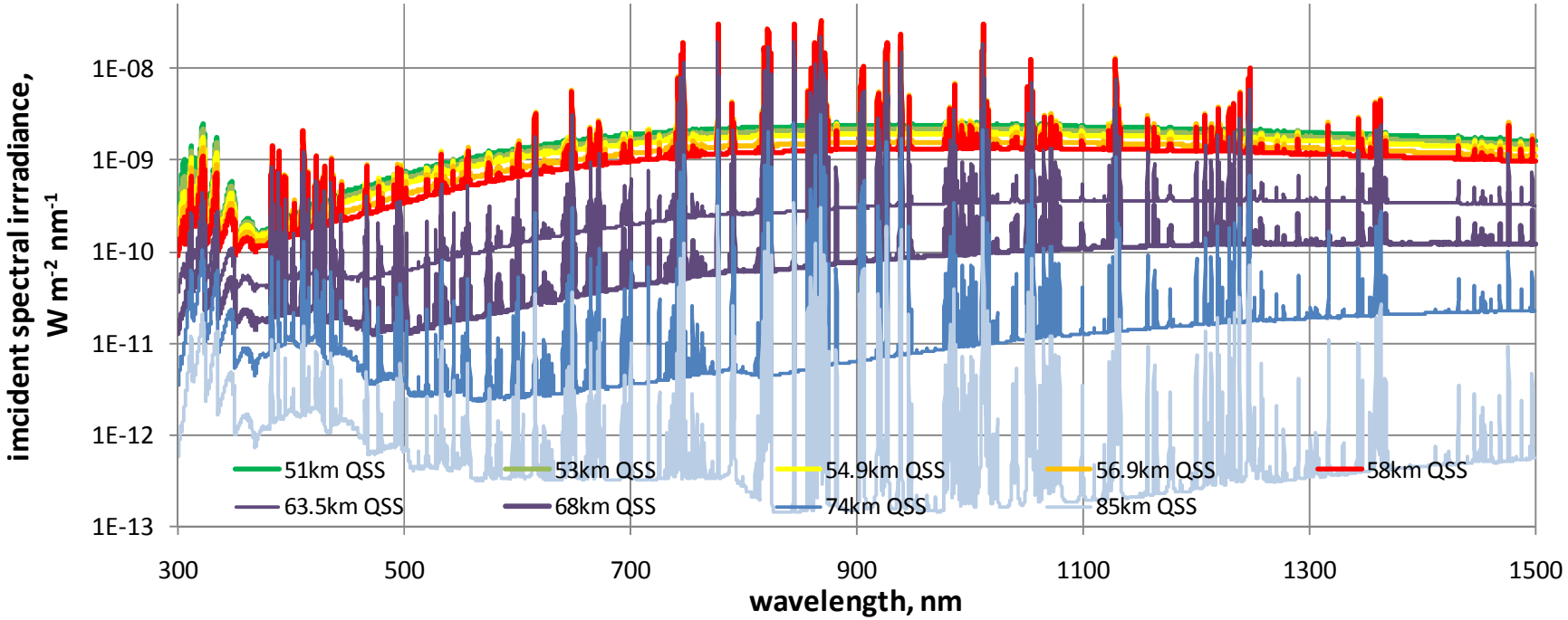

Combined thermal and plasma emission in high spectral resolution (HWFM 0.3nm)

Incident Radiation

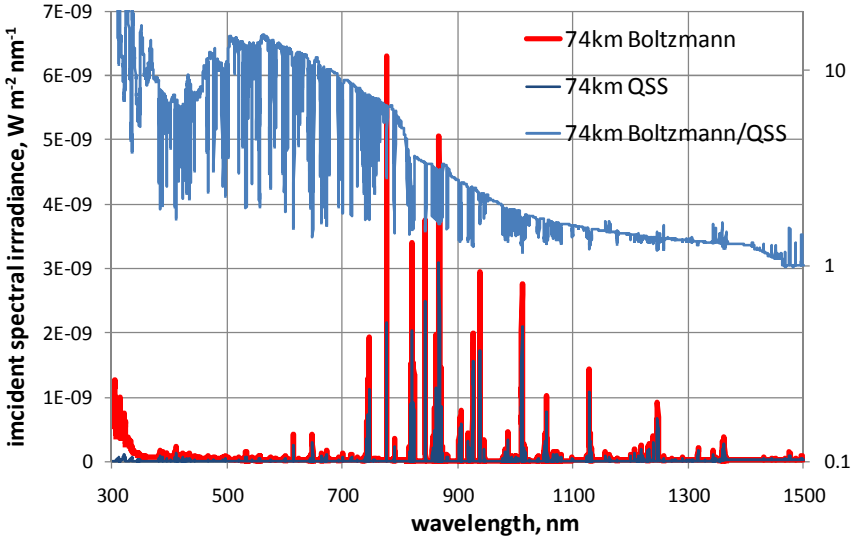

- At high altitudes, Boltzmann distributions yield remarkably higher plasma intensities than QSS.
- At peak radiation heating, some atom line peak intensities are higher with QSS than with Boltzmann; at lower altitudes almost all.
- The oxygen line triplet at 777nm and the molecular emission, however, are always stronger with Boltzmann.

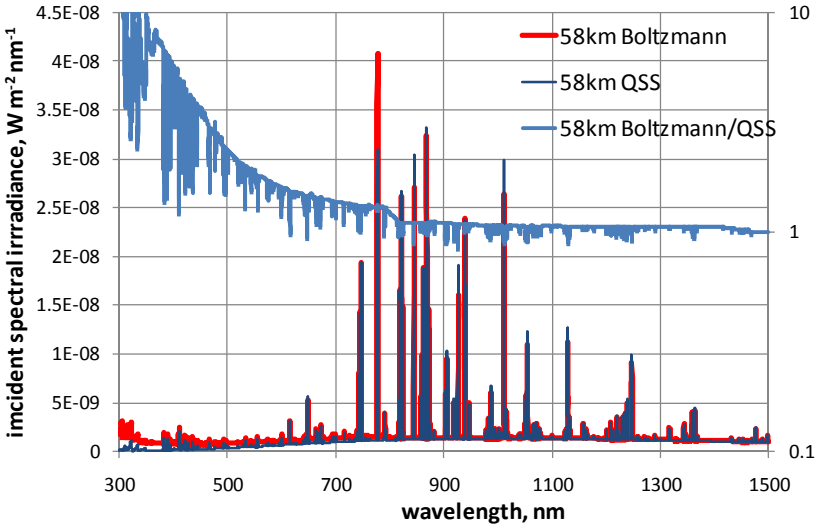

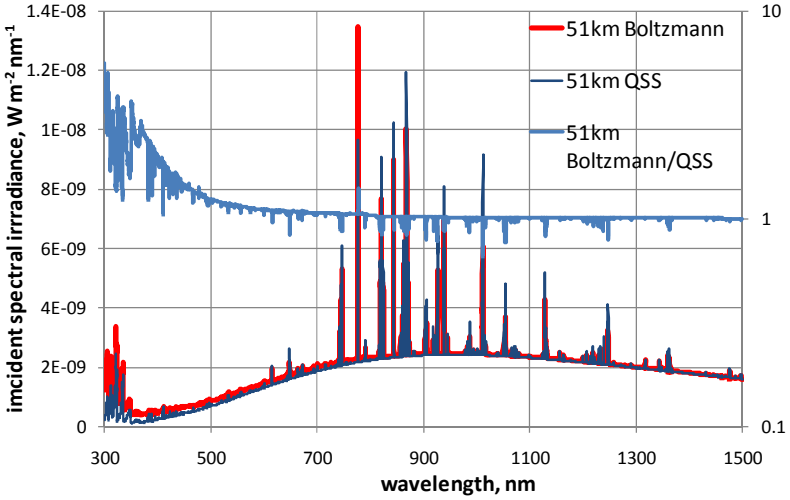

Incident Radiation

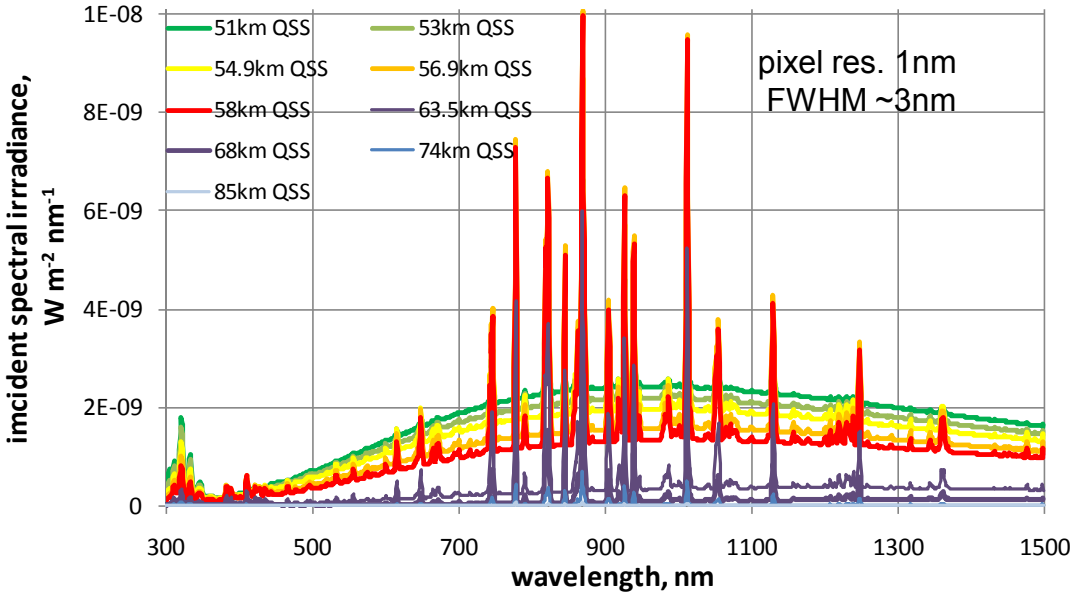

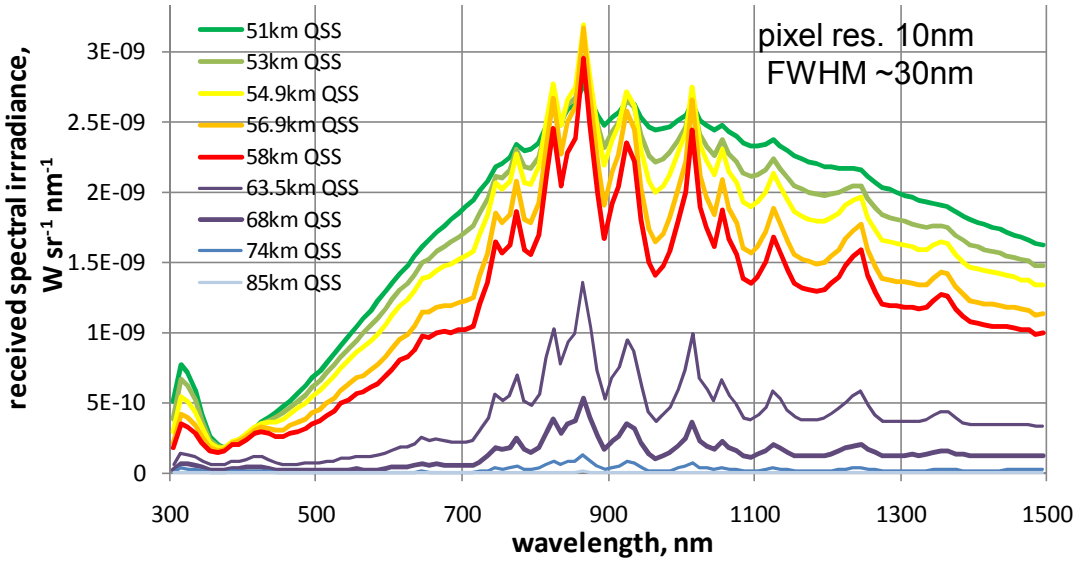

- For time reasons and due to missing broadening information of the experimental data, no explicit computations of spectra in low resolution have been performed yet.

- Instead, the high resolution spectra were integrated and averaged to estimate spectra in lower resolution.

Calibration

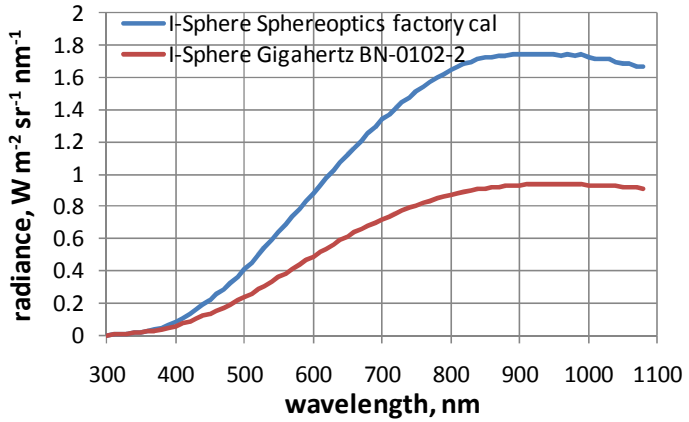

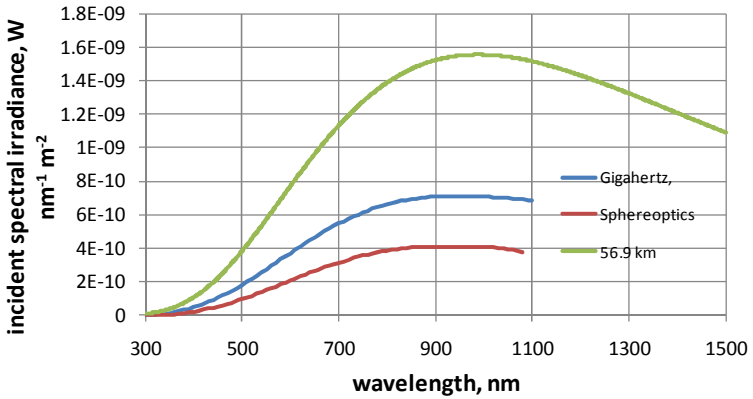

- Two different I-spheres used in ~29 m distance to the airplane used with apertures of 0.5 and 0.8 mm → radiation source of the same order of magnitude as anticipated during reentry based on pre-flight CFD estimates at peak heating at 56.9km
- Post-flight analysis shows thermal radiation at peak heating higher by a factor of 2
- measured during calibration:
  - distance lamp to each DC-8 window by laser distance meter
  - distance of entrance aperture to window
- in addition, post-flight check of aperture size (only large aperture so far → 809μm)

Info for PIs:

- Factory recalibration for the Sphereoptics I-sphere available. Please check!
- Please send in individual distances entrance aperture – window
- Data file with calibration data including radiance/irradiance conversion can be provided. Contact Michael.Winter@nasa.gov .

How to proceed?

- The current results are considered preliminary until more detailed sensitivity studies have shown that the spectral resolution in *NEQAIR* as well as the parameters used for the extraction of the lines of sight were sufficiently well chosen.
- A new set of atomic line constants is in preparation to be implemented into *NEQAIR*. As soon as these data are available, the results will be recomputed.

- For a comparison with experimental data, the individual wavelength increments and line broadening parameters of the set-up of concern have to be communicated to NASA to provide individually tailored simulation data.

- A re-computation of the flow field with surface blowing and ablation product chemistry seems desirable to be able to compare with the major molecular radiators in the experimental data (i.e. CN) and other ablation products (e.g. H).
DPLR is able to handle surface blowing but the inclusion of ablation chemistry in the flow field has yet to be finally implemented.

Thank you!
Happy to answer

Questions ?

Stagnation Line

expected equilibrium region

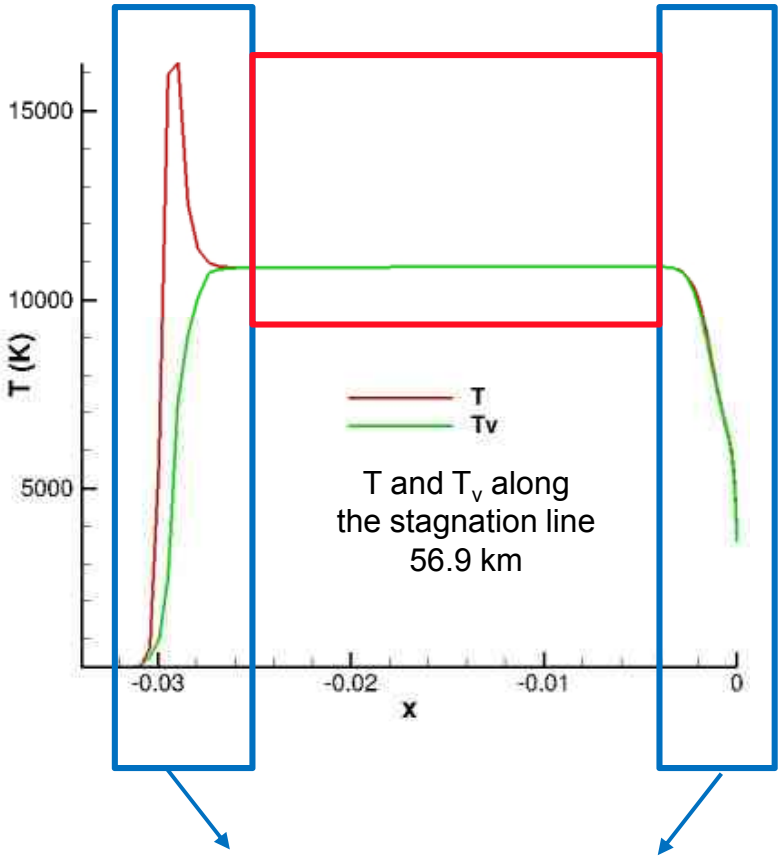

non-equilibrium radiation expected

expected equilibrium region

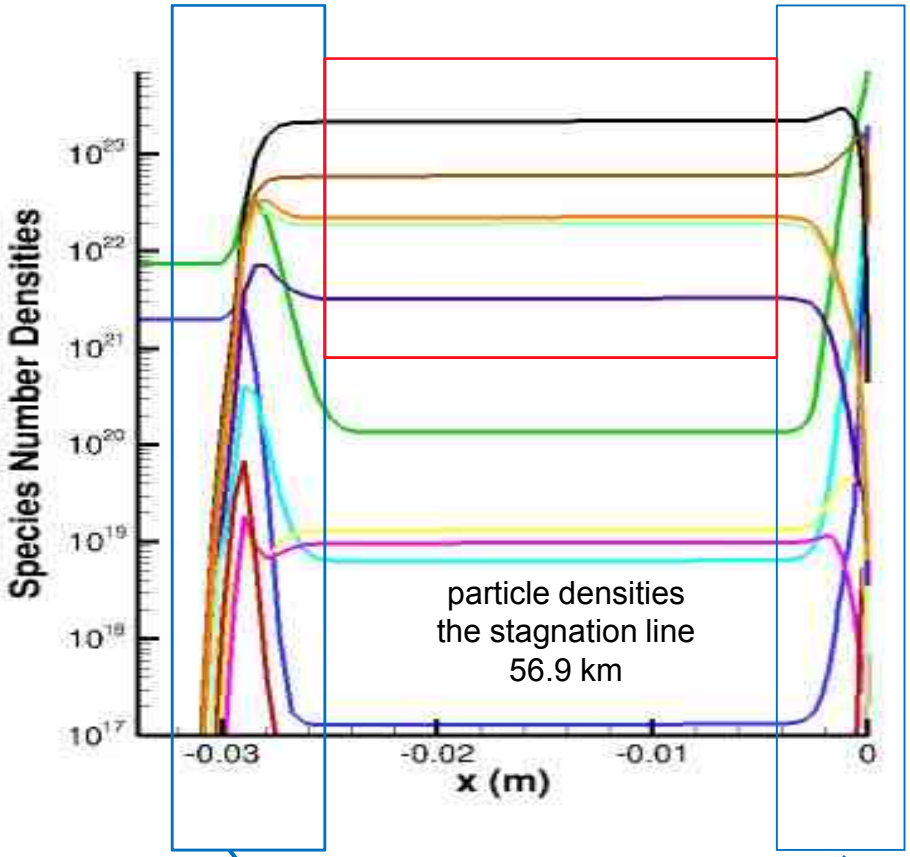

non-equilibrium radiation expected